JOURNAL OF MATERIALS SCIENCE 29 (1994) 2297–2303

An acousto-ultrasonic study of the effect of porosity on a sintered glass system

B. O. ADUDA, R. D. RAWLINGS
Department of Materials, Imperial College of Science, Technology and Medicine, London SW7 2BP, UK

An assessment of the applicability of an acousto-ultrasonic (AU) technique for the monitoring of porous ceramic systems has been carried out. Sintered glass was used as a model system and it was found that the AU parameters, such as normalized ringdown count, normalized pulse width, velocity and frequency interval (Δf) between adjacent peaks in the frequency spectra, decrease with increasing porosity. The porosity dependence of the normalized AU parameters has been attributed to attenuation which analysis showed depended on the pore size and content. The velocity and frequency interval changes also depended on pore content but, unlike the normalized parameters, were found to be sensitive to pore shape and size. The decreasing Δf with increasing porosity was explained in terms of the longer path lengths traversed by the waves in the higher pore-density samples.

1. Introduction

Acousto-ultrasonics (AU) is a relatively recent non-destructive evaluation (NDE) method in which elastic waves are injected into the specimen or component under test by a transmitting transducer and the modulated output picked up by a second (receiver) transducer and analysed using various signal analysis techniques. The monitored AU signals thus reflect the global effect of the volume of material between the test transducers on the stress waves [1].

In the analysis of the AU signals two main approaches have been employed: (i) similar methods as used in acoustic emission (AE) monitoring such as ringdown counting and (ii) calculating the spectral moments from the frequency spectrum domain [2, 3]. The quantified AU signal is often referred to as the "stress wave factor" and this is considered an indication of the efficiency of energy propagation in the material [1, 4] or a measure of the energy associated with the particular mode of propagation [5]. Energy or wave propagation will be affected by the presence of defects which in turn determine mechanical performance. AU has been most widely applied to polymer matrix composites and the stress wave factor has been found to correlate well with strength (e.g. [6]).

Since AU is not designed to locate and size individual flaws but to assess quantitatively the overall condition of the material between the two tranducers it should be especially suited for monitoring ceramic or ceramic-matrix composites (CMCs) in which the flaws are usually very small, numerous and well distributed. Given the relative dearth of NDE methods for ceramics and CMCs, and the current upsurge in interest in ceramic structural components, it is surprising that studies on the assessment of the applicability of AU to these materials are scarce. Nevertheless it has been shown that AU can be used to monitor crystallization in a glass–ceramic [7], porosity and strength of porous gypsum [8], and the thermal shock behaviour of alumina and zirconia-toughened alumina [9].

The work reported here was instituted in order to obtain a better understanding of the basic principles of the monitoring of the quality of ceramics by AU. Sintered glass compacts have been used as a model system and the effects of porosity on a number of acousto-ultrasonic parameters, such as the normalized ringdown count and the frequency spectra, have been investigated. The results have been interpreted in terms of theoretical attenuation based on the porosity content and pore size obtained from microstructural examination.

2. Experimental procedure

2.1. Glass powder and sintering

The glass powder used in the study was "impact glass beads" (Ballotini Ltd, UK) whose theoretical density was $2.47 \pm 0.02\ \mathrm{Mg\,m^{-3}}$. Three different batches of powder (designated BL, AD and AH) with different particle size distributions were employed. The particle size distribution of batch BL was determined by image analysis and that for AD and AH by a laser diffraction method. The nominal size distribution range and mean particle size of the batches were: BL, 45–1000 and 500 μm; AD, 106–250 and 170 μm; AH, 45–106 and 60 μm. The packing density of the three powders as a percentage of the theoretical density was 63.5, 63.4 and 63.9% for BL, AD and AH, respectively.

Sintering was carried out in a spherical graphite mould of 20 mm diameter and in an argon atmosphere. The heating rate to the sintering temperature of 708 °C was $5\ ^{\circ}\mathrm{C\,min^{-1}}$ and the time at tempera-

ture was varied to produce a range of porosities and microstructures.

2.2. Acousto-ultrasonic measurements

AU assessment (stress wave factor, velocity measurement and spectral analysis) of the sintered glass compacts was performed using standard AE equipment with a pulsing unit to which was added a waveform digitizer and spectrum analyser (Fig. 1). Two pairs of transducers were used as the transmitter and receiver. The first set, hereafter designated type B, had a frequency range of 100–300 kHz and a resonant frequency of 150 kHz whereas the second set (designated type S) had a wider frequency range of 100–1000 kHz. The transducers were coupled to the samples by a thin sheet of elastomer; use of this dry couplant eliminated any risk of contamination of the porous samples that would have occurred with the more conventional wet couplants.

50 pulses, at a repetition rate of one pulse per second, were injected into the specimens and the cumulative ringdown count, the pulse width (duration) and the averaged time-domain waveform and the corresponding spectrum recorded. This procedure was repeated three times for each loading of the specimen in the test rig. A specimen was loaded into the rig at least three times and thus each data point represents an average of a least nine readings. The propagation velocity of the stress waves in the specimen was obtained from the transit time (as measured from the time domain) and the dimensions of the specimen.

2.3. Density, porosity and microstructural studies

Samples were mounted and polished to a 1 μm finish for microstructural examination. Image analysis (lineal method) was performed on selected samples to obtain the pore size distribution. At least 300 chord lengths were measured and the number frequencies of the chord lengths were converted into pore size distribution from plots of cumulative frequency versus chord length using the relationship [10]

$$N(D) = \frac{2N(L)}{\pi L^2} - \frac{2(\mathrm{d}N(L)/\mathrm{d}L)}{\pi L} \quad (1)$$

where $N(D)$ is the number of pores per unit volume with diameters between D and $D + \mathrm{d}D$, and $N(L)$ is the measured number of chords per unit length in the size range L to $L + \mathrm{d}L$ in the planar section of the sample. Fig. 2 gives a typical pore length distribution and Fig. 3 the pore size per unit volume against chord length plot obtained using this procedure. Representative micrographs are presented in Fig. 4 for a BL

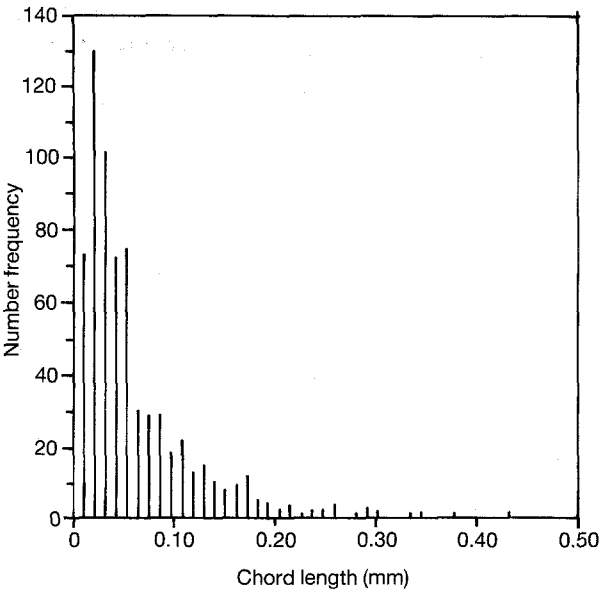

Figure 2 Typical distribution of chord lengths of pores in a sintered glass compact (AD compact with $P = 14.8\%$).

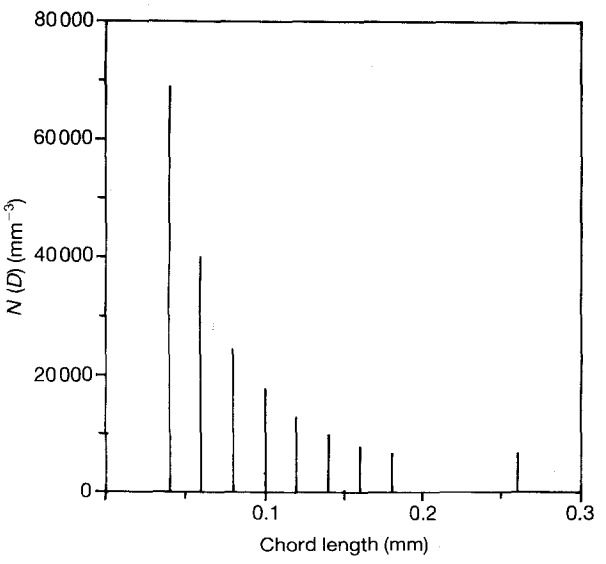

Figure 3 Typical plot of number of pores per unit volume $N(D)$ versus chord length for a sintered glass compact (AD compact with $P = 14.8\%$).

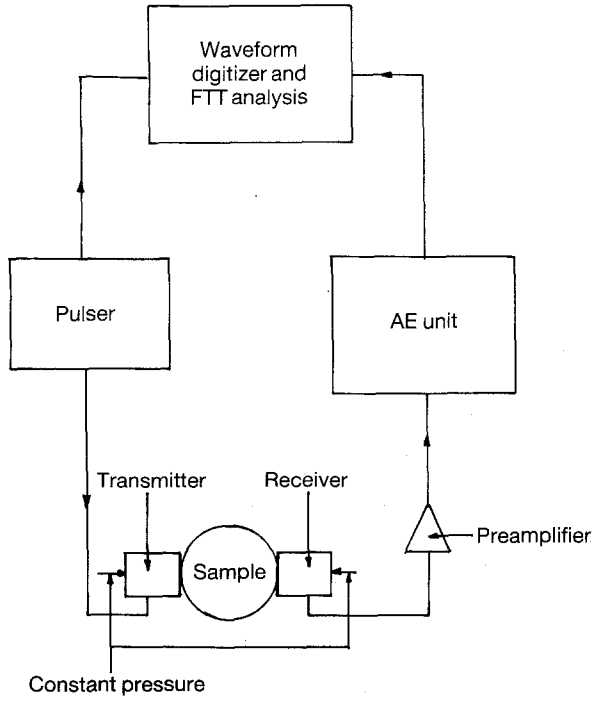

Figure 1 Schematic diagram of the apparatus for acousto-ultrasonic testing.

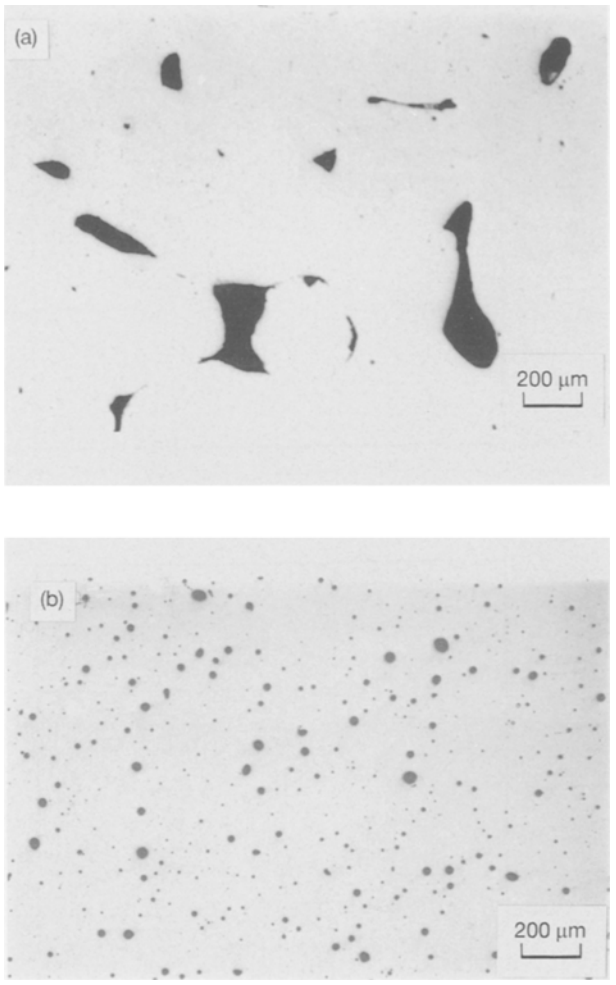

Figure 4 Micrographs of sintered glass compacts showing the differences in pore size, shape and content: (a) BL compact with $P = 13.0\%$, (b) AH compact with $P = 8.3\%$.

compact with 13% porosity and an AH compact with 8.3% porosity; note the spherical pores in the latter.

The bulk density ρ_b was measured using the Archimedes principle and the porosity P (%) calculated from the relation

$$P = \left(1 - \frac{\rho_b}{\rho_g}\right)100 \qquad (2)$$

where ρ_g is the theoretical density of the glass.

The open pore size distribution of selected samples was determined using a mercury porosimeter and following standard procedures. Characteristic open pore size distributions are shown in Fig. 5 for an AD compact with $P = 14.8\%$ and an AH compact with $P = 22.5\%$.

3. Results

The normalized cumulative ringdown count (CRDC) and pulse width fall as porosity increases and, as exemplified by the normalized CRDC data of Fig. 6, are independent of the type of transducer and equipment settings used. The normalization factor used was the maximum AU parameter value obtained with the respective sets of transducers. The normalized parameters as a function of porosity are shown in Fig. 7 for

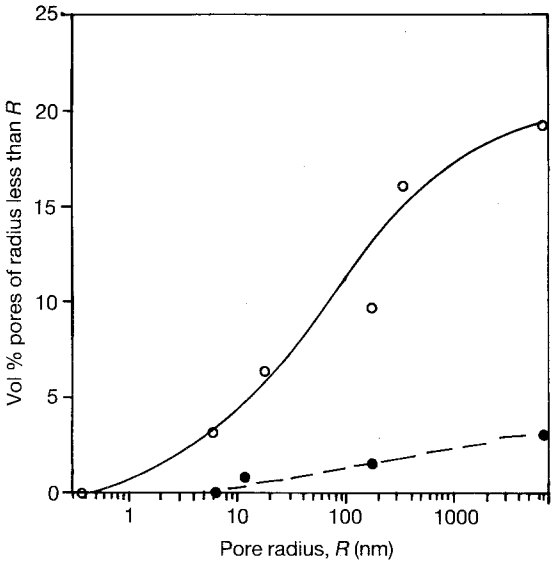

Figure 5 Open pore size distributions for sintered glass compacts: (○) AD ($P = 14.8\%$), (●) AH ($P = 22.5\%$).

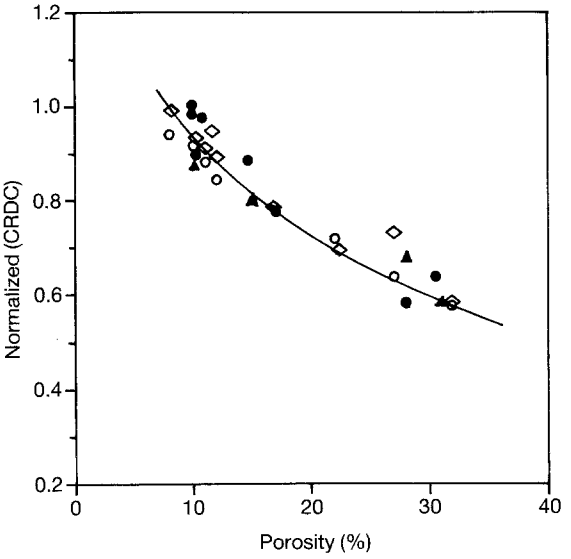

Figure 6 Plot of normalized CRDC versus pore content for AD and AH compacts using both type B and type S transducers: (●) batch AD (S), (▲) batch AD (B), (○) batch AH (B), (◇) batch AH (S).

BL compacts and Fig. 8 for AD and AH compacts. It can be seen that the normalized parameters are the same, within experimental error, for AD and AH but different for BL compacts. The variation in velocity with porosity (Fig. 9) exhibited a similar decrement pattern as the other AU parameters but did not distinguish between compacts made from batch BL and those from batches AD and AH.

The waveforms were sensitive to porosity content as demonstrated by the typical waveforms, and their corresponding frequency spectra, for some BL compacts in Fig. 10. Particularly noticeable is the progressive increase in the number of peaks in the frequency spectra as porosity increases. Furthermore, at the higher porosities the peaks begin to overlap and consequently the troughs (minimum-to-maximum heights) are smaller. The same general features and trends were observed for compacts produced from

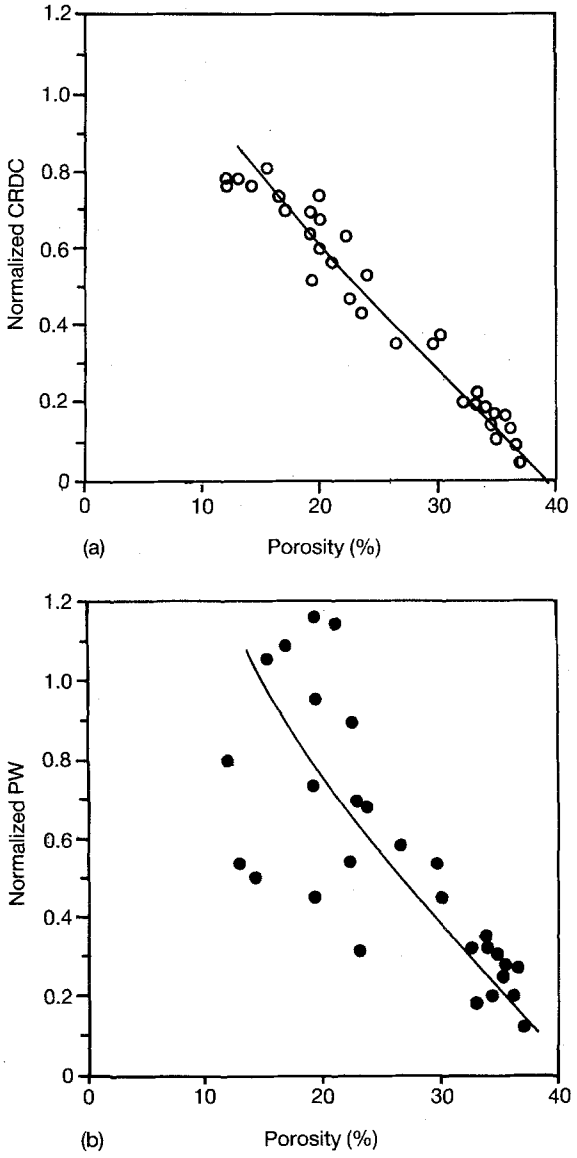

Figure 7 Plots of normalized AU parameters versus pore content for BL compacts (type B transducer used): (a) CRDC, (b) pulse width, (PW).

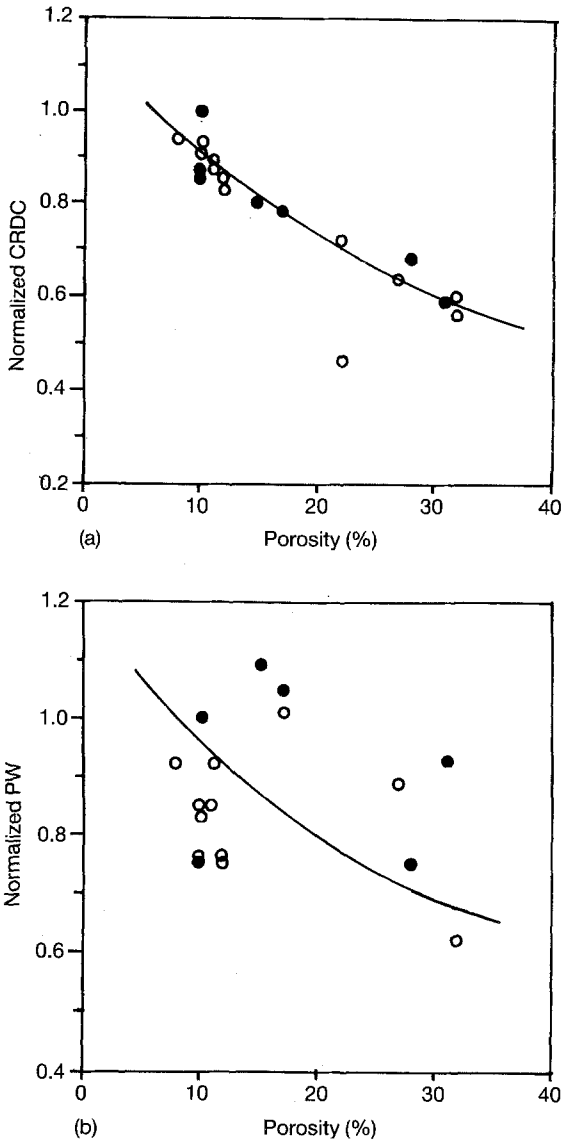

Figure 8 Plots of normalized AU parameters versus pore content for (●) AD and (○) AH compacts (type S transducer used): (a) CRDC, (b) pulse width (PW).

batches AD and AH. The average frequency interval (Δf) between adjacent peaks for each type of compact is shown in Fig. 11. The decrease in Δf with increasing porosity is, like the velocity, independent of the starting powder.

4. Discussion

The fall in the AU parameters with increasing porosity is attributed to attenuation caused by scattering of the stress waves. This is illustrated in Fig. 12 (normalized cumulative ringdown count for some glass compacts are inset), in which the theoretical attenuation has been calculated from the relation [11].

$$\alpha_S = \frac{N(\Omega)}{2}\Omega \qquad (3)$$

where α_S is the attenuation due to scattering, $N(\Omega)$ the number of scatterers per unit volume and Ω the scattering cross-section. Equation 3 is valid as long as the scatterers are independent (non-interacting). In the

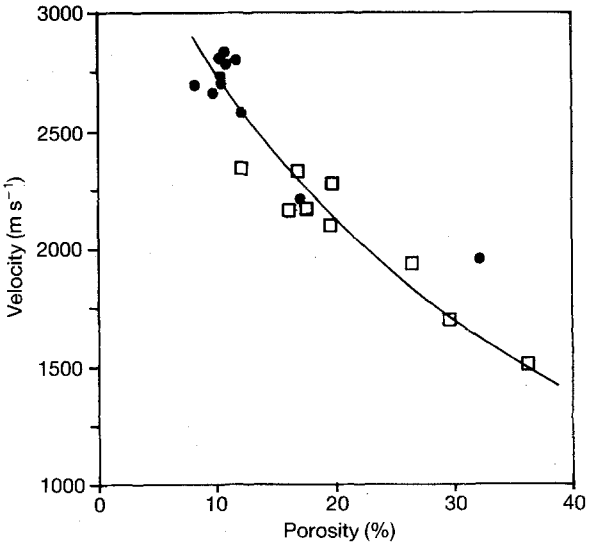

Figure 9 Graph showing that the porosity dependence of the velocity is the same for all compacts: (●) AD and AH, (□) BL.

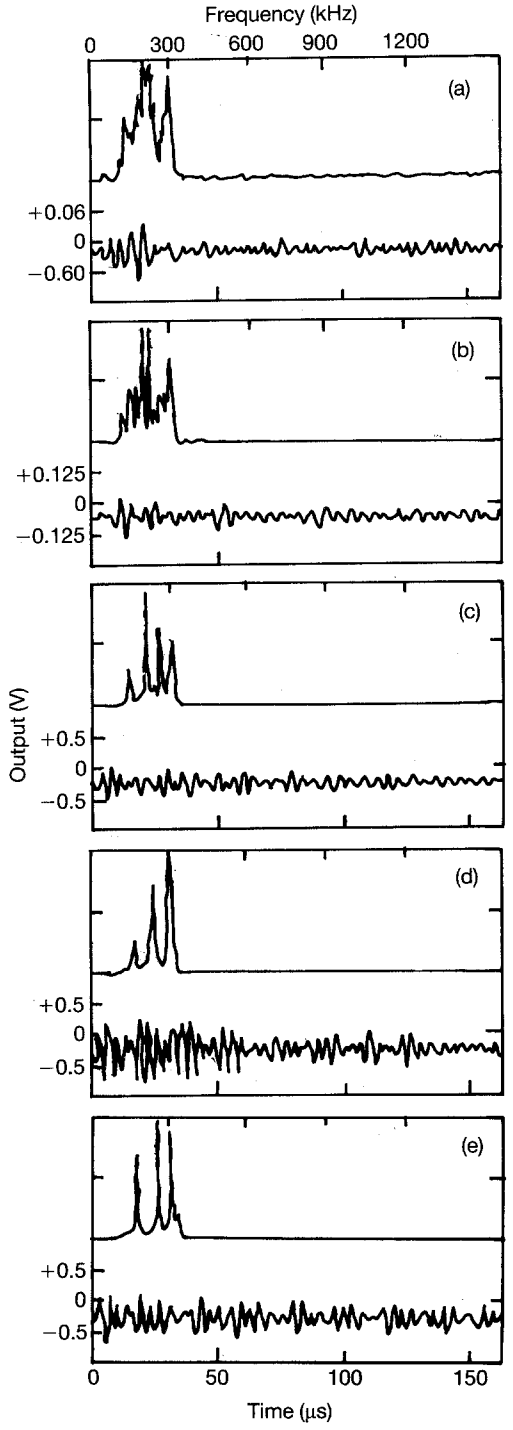

Figure 10 Frequency spectra (upper) and waveforms (lower) of BL compacts of different pore contents: (a) $P = 36.1\%$ (b) $P = 32.8\%$ (c) $P = 19.3\%$ (d) $P = 16.4\%$ and (e) $P = 12.3\%$.

Rayleigh scattering region ($\lambda \gg D$, where λ is the wavelength and D the size of the scatterer) the scattering cross-section (Ω) for a cavity is given by the relation suggested by Truel *et al.* [11]:

$$\Omega = \frac{4}{9} g_c (\kappa_1 D)^4 \qquad (4)$$

where g_c is a constant given in terms of the longitudinal wave number (κ_1) and the transverse wave number (κ_2).

In the present study the number of scatterers (pores) per unit volume $N(D)$ was obtained from the microstructure through Equation 1. The validity of the

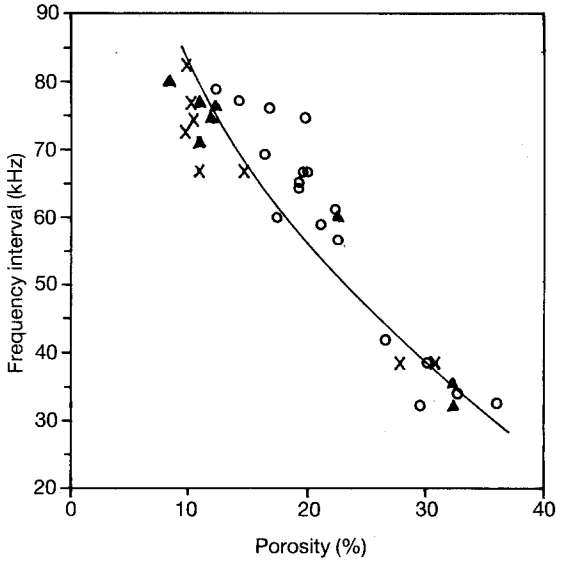

Figure 11 Graph showing that the porosity dependence of the average frequency interval (Δf) between adjacent peaks in the spectra is the same for all compacts: (×) AD, (▲) AH, (○) BL.

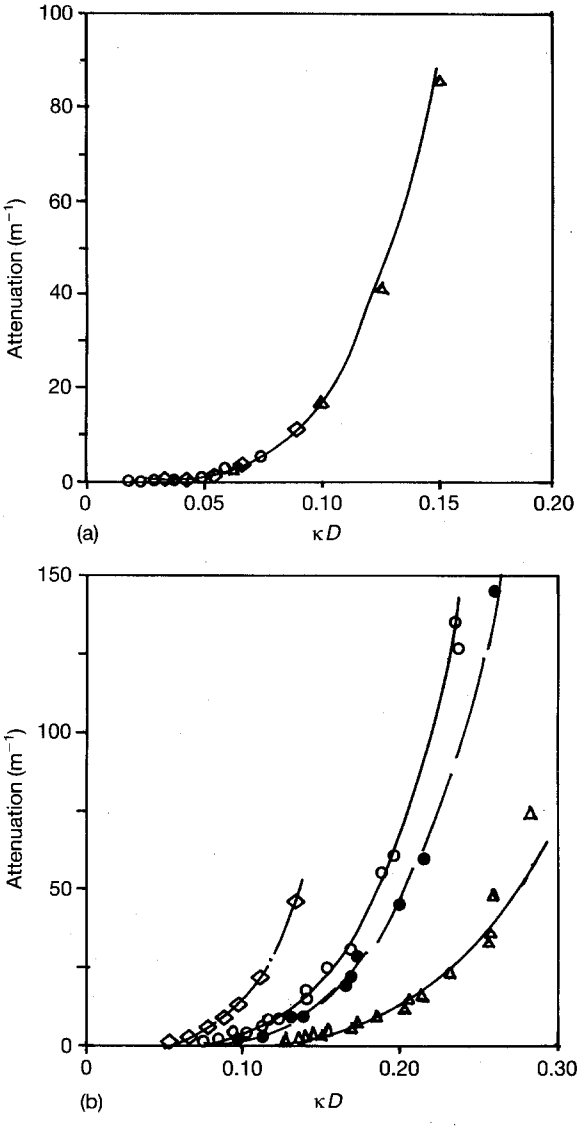

Figure 12 Theoretical attenuation of glass compacts as a function of normalized pore size (κD) where κ is the wave number and D is pore size: (a) AD and AH compacts of porosity and normalized CRDC of (◇) 12.2% and 0.85, (△) 17.1% and 0.72, (○) 22.5% and 0.78; (b) BL compacts of porosity and normalized CRDC of (●) 23.3% and 0.45, (◇) 13.3% and 0.78; (○) 23.9% and 0.53, (△) 13.0% and 0.77.

Rayleigh condition was tested using the expression of Lefebvre *et al.* [12]:

$$\frac{N(D)}{\kappa_1}\Omega \ll 1 \tag{5}$$

and assuming the following: longitudinal velocity of sound in the glass compacts = 2500 m s^{-1}, $\kappa_1/\kappa_2 = 2^{1/2}$, frequency range 100–300 kHz. With these assumptions, and $N(D)$ values obtained using Equation 1, Equation 5 yielded values between 69.0×10^{-8} and 0.74. Apart from the 0.74 value, all values were ≤ 0.2, thus confirming that the Rayleigh conditions were obeyed for the glass compacts with porosity less than 25%. It should be pointed out that although the velocity changes with porosity (see Fig. 9), assuming a single value for the calculations did not result in significant errors.

Fig. 12 demonstrates that attenuation increases with the pore size. The data for AD and AH compacts lie on a single curve (Fig. 12a) and comparison with Figs 8 and 9 shows that samples with higher attenuation have correspondingly lower AU parameters. The data for BL compacts do not fall on a single curve and do not follow a regular sequence with porosity content (Fig. 12b), although no significant anomalies were observed in the porosity dependence of the AU parameters. The cause of this difference stems from the fact that in the former samples (AD and AH) the pores, as shown in the micrograph of Fig. 4, were more spherical than in the latter, and hence the results for the AD and AH compacts were in better agreement with the model since in the derivation of Equation 4 spherical pores (cavities) have been assumed.

If the variation with porosity of the normalized AU parameters, in particular the normalized CRDC, is compared with the variation in mechanical properties with porosity reported in the literature [13], it can be seen that the trend is similar. Since the same features, namely the pores, affect the propagation of ultrasound in the sintered glass also determine the mechanical properties, e.g. they act as flaws for the initiation of fracture, it is reasonable to apply the empirical relations or those derived theoretically (based on dynamic or static theories) to relate mechanical properties to the porosity content to the AU results. In this study we have used the empirical mechanical property relation [8, 14]

$$M = M_0(1 - \beta P)^n \tag{6}$$

where M is the mechanical property at porosity P, M_0 is the mechanical property at zero porosity, β is a grain-packing geometry pattern factor ($1 \leq \beta \leq 3.85$) and n is a measure of the spherical nature of the pores, but with M replaced by an AU parameter. Similarly in the theoretical model of Kerner [15]:

$$\tilde{M} = \frac{K(1 - P)}{1 + 3(KP/4\mu)} + \frac{(4/3)\mu}{1 + \{15(1 - \nu)P/[(7 - 5\nu)(1 - P)]\}} \tag{7}$$

where $\tilde{M}$ is the effective mechanical property of the porous material, ν the Poisson's ratio and μ the Lame's constant. Fig. 13 shows the normalized CRDC (experimental and also calculated from Equation 6) and the normalized mechanical property $\tilde{M}$ from Equation 7 as a function of porosity. From Equation 6 the values of β and n were 2.4, 1.33 and 1.25, 1.13 for BL compacts and AD and AH compacts, respectively. These values of β indicate that in the compacts made from the large-particle BL batch a more orderly arrangement existed than in the compacts from batches AD and AH. This is consistent with the observation that in the batches AD and AH, a tendency towards particle agglomeration was very evident whereas no agglomeration was observed in batch BL. The slightly larger value for n for the BL compacts is consistent with the pores being less spherical than in AD and AH compacts.

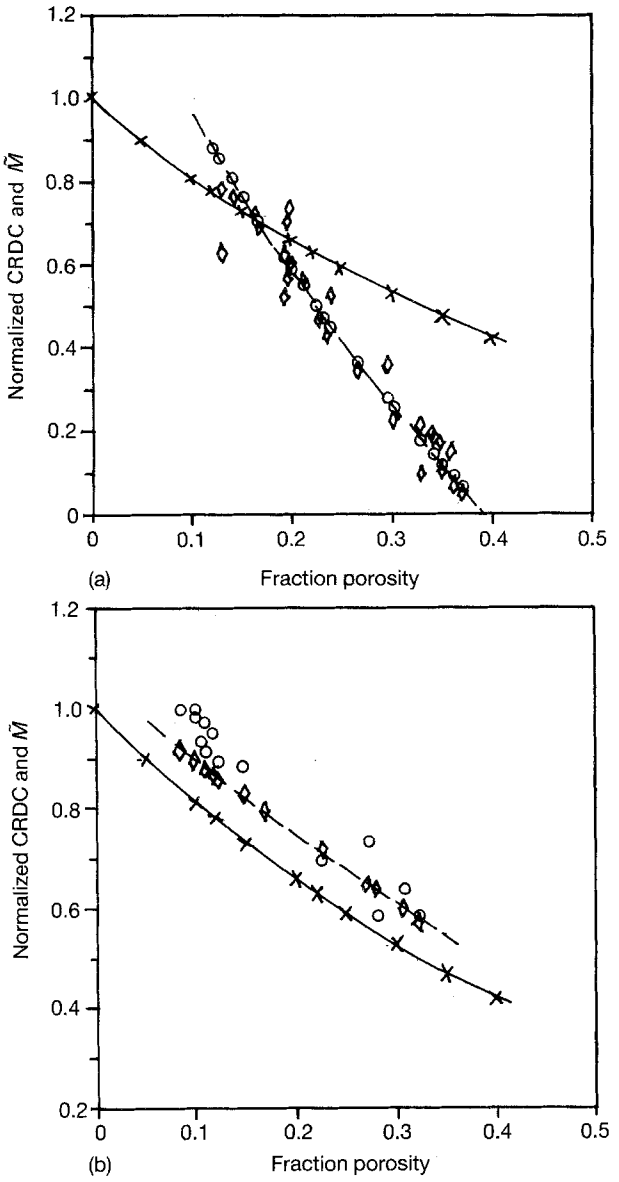

Figure 13 Variation with porosity of measured AU parameter (normalized CRDC), theoretical normalized CRDC calculated from Equation 6, and theoretical normalized mechanical property $\tilde{M}$ calculated from Equation 7. (a) BL compacts: (◇) experimental, (○) Equation 6, (×) Equation 7. (b) AH compacts: (○) experimental, (◇) Equation 6, (×) Equation 7.

The rapid decay of the waveforms as porosity increased further indicates that attenuation was significant at higher porosities. This also accounts for the modulation observed in the frequency spectra. It has been shown [15, 16] that if Δt is the delay time between waves received, then a maximum (peak) in the frequency spectrum will be centred at the frequency f_n given by

$$\Delta t = n/f_n \tag{8}$$

where n is an integer. From Equation 8 the frequency interval Δf between two adjacent peaks is given by

$$\Delta f = \frac{n+1}{\Delta t} - \frac{n}{\Delta t} = \frac{1}{\Delta t} \tag{9}$$

It follows from this that when Δt increases, the frequency interval decreases. We know that as porosity increases the time interval between the arrival of each signal at the transducer increases as some have travelled more tortuous paths and so have suffered longer time delays. It is this increasing of the time interval with porosity which accounts for the observed decrease in the frequency interval as porosity increases (Fig. 11). It is interesting to note that both velocity and Δf appear to be determined solely by the porosity content whereas the attenuation, as measured by the normalized ringdown count and pulse width, depends also on the pore size and shape. The diminishing difference from minima to maxima noted in the frequency spectra can be attributed to attenuation [15, 16].

5. Conclusions

1. The normalized acousto-ultrasonic parameters (ringdown count and pulse width), velocity and frequency interval between adjacent peaks in the spectra decreased with increasing porosity.

2. The dependence of the normalized AU parameters on porosity for the different batches of sintered compacts was satisfactorily described by modelling the effects of pore size and content on attenuation.

3. The decrease in the frequency interval Δf in the spectra with increasing porosity was accounted for by the more tortuous paths travelled by the waves at the higher pore densities. Δf and the wave velocity were found to be dependent on the porosity content but insensitive to pore size and shape.

4. AU shows promise as a non-destructive evaluation method for ceramic materials.

Acknowledgement

The authors thank the British Council for sponsoring the project.

References

1. K. K. PHANI and N. R. BOSE, *J. Mater. Sci.* **21** (1986) 3633.
2. M. T. KIERNAN and J. C. DUKE, *Mater. Eval.* **46** (1988) 1105.
3. R. TALREJA, in "Acousto-ultrasonics Theory and Applications", edited by J. C. Duke (Plenum, New York, 1988) p. 177.
4. A. VARY and R. F. LARK, *J. Test. Eval.* **7** (1979) 185.
5. J. C. DUKE, E. G. HENNEKE, M. T. KIERNAN and P. P. GROSSKOPF, "A study of the Stress Wave Factor Technique for Evaluation of Composite Materials", NASA Contractor Report 4195, Grant NAG3-172 (NASA, 1989).
6. J. C. DUKE (ed.) "Acousto-ultrasonics Theory and Applications", (Plenum, New York, 1988).
7. A. De, K. K. PHANI and S. KUMAR, *J. Mater. Sci. Lett.* **6** (1987) 17.
8. K. K. PHANI, S. S. NIYOGI, A. K. MAITRA and M. ROYCHAUDHARY, *J. Mater. Sci.* **21** (1986) 4335.
9. I. THOMPSON and R. D. RAWLINGS, *ibid.* **26** (1991) 4534.
10. E. E. UNDERWOOD, A. R. COLCORD and R. C. WAUGH, in "Ceramic Microstructures, their Analysis, Significance and Production", edited by R. M. Fulrath and J. A. Pask (Wiley, New York, 1968) p. 25.
11. R. TRUEL, C. ELBAUM and B. B. CHICK, "Ultrasonic Methods in Solid State Physics" (Academic, New York, 1969) p. 172.
12. J. LEFEBVRE, J. FROHLY, R. TORGUET, C. BRUNEEL and J. M. ROUVAEN, *Ultrasonics* **18** (July 1980) 170.
13. L. CORONEL, J. P. JERNOT and F. OSTERSTOCK, *J. Mater. Sci.* **25** (1990) 4866.
14. K. K. PHANI and S. K. NIYOGI, in "High Tech Ceramics", edited by P. Vincenzini (Elsevier, Amsterdam, 1987) p. 1391.
15. W. A. SIMPSON, *J. Acoust. Soc. Amer.* **56** (1974) 1776.
16. H. E. KAUTZ, in "Acousto-ultrasonics Theory and Applications", edited by J. C. Duke (Plenum, New York, 1988) p. 127.

Received 16 September
and accepted 8 October 1993